Available online at www.sciencedirect.com
ScienceDirect
Journal of Power Sources 176 (2008) 452–459
JOURNAL OF POWER SOURCES
www.elsevier.com/locate/jpowsour

Combined neutron radiography and locally resolved current density measurements of operating PEM fuel cells

Ch. Hartnig [a,*], I. Manke [b,d], N. Kardjilov [b], A. Hilger [b,c], M. Grünerbel [a], J. Kaczerowski [a], J. Banhart [b,d], W. Lehnert [a]

[a] *Centre for Solar Energy and Hydrogen Research (ZSW), Ulm, Germany*
[b] *Hahn-Meitner Institute (HMI), SF3 Berlin, Germany*
[c] *University of Applied Sciences (TFH) Berlin, FB II, Germany*
[d] *Technical University Berlin, Faculty 3, Germany*

Available online 28 August 2007

Abstract

Neutron radiographic imaging is combined with locally resolved current density measurements to study the effects of local water content on the performance of the corresponding electrochemical active area in an operating PEM fuel cell. Liquid water agglomerates are detected, quantified and correlated with the activity of the respective area. At low currents, depletion of the reactant gas leads to a decreasing performance along the anodic flowfield channel. At high currents, an optimum humidification is reached in the central part of the fuel cell; close to the inlets respectively outlets, flooding and drying can be observed concurrently and cause a non-uniform current density distribution across the reactive area. The fast response of the local performance on water droplets migrating in the gas channel is tracked by short-term imaging taking place on a timescale of several seconds.

Keywords: PEM fuel cell; Neutron imaging; Water management; Locally resolved current density

1. Introduction

The worldwide energy demand and the rapid approach of 'peak oil', which is expected to be reached within this decade and results in an overall decreasing production of crude oil, require a drastic change towards highly efficient energy conversion systems and regenerative sources. Fuel cells bear the potential for applications as automotive as well as residential power supplies. Among several types of fuel cells, low temperature polymer electrolyte membrane fuel cells (PEMFC) are considered for a wide range from mobile to portable as well as stationary applications. Besides financial aspects such as the overall price the long-term stability is still an issue, which has to be solved properly to achieve a broad market penetration of these devices. A key task to clarify the aforementioned technical problems is a proper water management of the system; a minimum humidity inside the cell is necessary for the membrane as a dry polymer undergoes structural changes resulting in a vanishing protonic conductivity. On the other hand, excess liquid water in the gas diffusion layer (GDL) or the flow field channels hinders the gas transport and therefore the supply of reactants to the catalyst layer.

During the last years, different experimental techniques were applied to study the transport of liquid water inside the flow field: several groups employed transparent components to monitor optically the formation of liquid water. Weng et al. [1,2] and Ma and coworkers [3] observed flooding effects on the cathode of PEM fuel cells and deduced from these observations impacts on the overall performance of the cell. This method has also been applied to direct methanol fuel cells by Scott and coworkers [4] and Zhao and coworkers [5] targeting for an optimized carbon dioxide management, which is one of the key factors for a highly efficient DMFC.

Further experiments extended the optical detection of liquid water by spatially resolved current density measurements. Hebling and coworkers [6,7] evaluated simultaneously current, temperature and water distribution inside the cell by means of transparent end plates. A further improvement was reached by an

* Corresponding author. Tel.: +49 731 9530 403; fax: +49 731 9530 666.
E-mail address: christoph.hartnig@zsw-bw.de (Ch. Hartnig).

0378-7753/$ – see front matter © 2007 Elsevier B.V. All rights reserved.
doi:10.1016/j.jpowsour.2007.08.058

additional measurement of the local electrical impedance spectra [8]. Spatially resolved information of the current density has been reported by means of different techniques, either a segmented flow field [9], respectively collector plate [10], or via an array of shunt resistors [11] embedded in the current collector plate. By either approach the water distribution and transport inside the PEFC can be studied in detail.

Common to the aforementioned techniques is the strong disturbance of the fuel cell setup with regard to electrical or thermal conductivity. The first attempts to study an unmodified and therefore undisturbed system were achieved by means of neutron radiography. This method is based on the high attenuation coefficient of hydrogen compared to one of the most metals; the neutron beam can penetrate the metallic housing of the cell as well as the graphitic or metallic flowfields almost unattenuated whereas liquid water leads to a strong absorption of the beam which allows for a detection of liquid water down to several nanoliter with a spatial resolution of down to 100 μm. This method was engaged by a number of groups [12–15] to detect liquid water in an unmodified fuel cell. First studies of material variations proved the method as suitable tool for target-oriented material development [16].

Recently, Scherer and coworkers combined the direct observation of liquid water with locally resolved impedance measurements and demonstrated that in a fuel cell driven in co-flow mode drying and flooding might be observed simultaneously, depending on the respective section of the PEMFC [17].

In this article we report combined neutron radiography studies with locally resolved current density measurements; this combination allows for a direct observation of liquid water and includes information on the local performance of the cell at the time of imaging. The technical details and the neutron radiographic setup are explained in the following section; a detailed analysis and the correlation between the amount of water and the local performance are explained in Section 3. In the conclusion, attempts towards a more uniform current distribution will be sketched.

2. Instrumentation and experiment

2.1. Radiography setup

The radiography experiments were performed at the neutron tomography instrument CONRAD/V7 at Hahn-Meitner Institute (HMI). It is located in the neutron guide hall of the research reactor BER-2 where low-energy neutrons (so-called cold neutrons) are used for experimental purposes. The radiography instrument is based on a pinhole geometry with a small variable aperture placed at the end of the neutron guide followed by a converged collimator with a length of 5 m toward the sample position. In this way, a well-collimated neutron beam is directed to the sample. The transmitted beam is detected behind the sample by a position sensitive detector. The main part of the detector system is the 16-bit low-noise CCD camera (Andor DW436N with 2048 × 2048 pixel), which is focused by a lens system on a neutron sensitive scintillator screen. To prevent any radiation damage of the camera, the image is deflected on a side under 90° by a mirror. The sample environment is equipped with a translation table, which allows to move the sample to the side and to take images of the unperturbed beam. This image is used further for normalization of the images with a sample in the beam. The normalization procedure helps to transform the gray levels from the radiography image to transmission values, which are the base for further quantitative analysis.

2.2. Fuel cell setup

A single cell setup has been used for the measurements. On the anodic and cathodic electrodes, a threefold serpentine flow field with 1 mm wide channels and ribs and an active area of 10 cm × 10 cm was applied. The flowfields were machined into graphite composite plates (SGL Carbon) with cooling flowfields on either electrode to ensure a proper thermostatization. GORE PRIMEA 5620 membrane electrode assemblies and SGL Carbon 10 BB material were employed in the fuel cell setup. The locally resolved current density was measured by means of shunt resistors embedded in a segmented multi-layer printed circuit board with a segment size of 4 cm^2; a more detailed description is given by Lehnert and coworkers [18]. The circuit board is attached in between the flow field and the end plate so that the local influence on the thermal and electrical conductivity of the components and the water development and transport in the cell is completely eliminated. Thus, this setup turns further modification or interventions of the cell redundant.

The fuel cell was fed in counter flow mode with hydrogen and humidified air (dew point 25 °C) with an anodic and cathodic utilization of 80%, respectively 25% at a cell temperature of 60 °C; the flowfield layout as well as the flow directions of the reactant gases together with the matrix for the current density measurement are given in Fig. 1. The overall current density i_0 of the galvanostatic measurements was varied in steps of 200 mA cm^{-2} from $i_0 = 700$ mA cm^{-2} to $i_0 = 100$ mA cm^{-2}. Here, special attention was payed to the two outmost values (700, respectively 100 mA cm^{-2}), as at high currents a high amount of water is produced whereas at low currents and the applied stoichiometry the removal of excess water is limited. Both conditions might lead to accumulation of excess water in the flowfields. At a current density of $i_0 = 700$ mA cm^{-2}, the potential could not be kept constant which gives a first hint on such effects.

Due to the epoxy substrate of the circuit board, a highly intensive neutron beam was necessary to transmit the plate and to achieve a good contrast for the small amount of water present in the GDL. Therefore, the maximum aperture of 3 cm was setup at the neutron radiography facility, which gives a spatial resolution of 500 μm at the sample position and a neutron flux of 2×10^7 neutrons cm^{-2} s. An exposure time of 0.2 s per image with a read out time of 1.8 s was applied to perform one radiography for every measured current density distribution. This way the time interval between two images in the image sequence taken in the experiment was 2.0 s in total. The timers of the circuit board and the radiography instrument were exactly aligned allowing to correlate the visual information of the water distri-

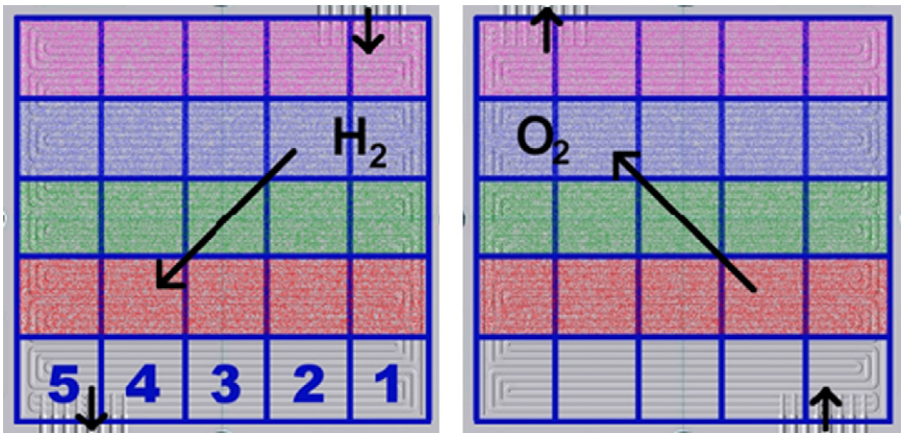

Fig. 1. Threefold serpentine flowfield layout and directions of reactant gas flow; left: anode, right: cathode. The segments of the printed circuit board are displayed; colors and numbering refer to the explanations given in the text (For interpretation of the references to color in this figure legend, the reader is referred to the web version of the article.).

bution in the cell with the two-dimensional distribution of the power output of the cell.

3. Results

The data processing was performed by a standard procedure: At first, the dark current signal was subtracted from the images, which were normalized further by using the unperturbed beam profile. In order to get quantitative information on changes of the water distribution in the cell a new renormalization of the image set was performed. Quotient images were calculated using the initial dry cell as a reference image for further division of the images taken at different operational conditions. In this way, only the contribution of the water distribution can be seen whereas all other details like cell geometry and beam inhomogeneity are removed in the resulting images. In Fig. 2a, an image as obtained from the experiment is displayed. The normalization of this image results in Fig. 2b where only the water is visible and all other components from the fuel cell are eliminated. In order to illustrate the current density distribution over the active area the respective segment fields of the circuit board have been colored according to the current density level and were added as overlays to the normalized radiographic images.

Long-term effects affecting the liquid water distribution were separated from quick responses of the cell performance by taking the average of ten radiographic images as well as the average of the current density. Thereby, contributions taking place on a short time scale (covered by single images) and effects of small droplets inside the gas diffusion layer were neglected; these effects will be discussed further below in more detail. Averaging the images results in an integral presentation of changes taking place within 20 s.

In Fig. 3a two normalized radiographic images with their respective current density distributions at an overall current density of $i_0 = 100\,\mathrm{mA\,cm^{-2}}$ are displayed. The liquid water is

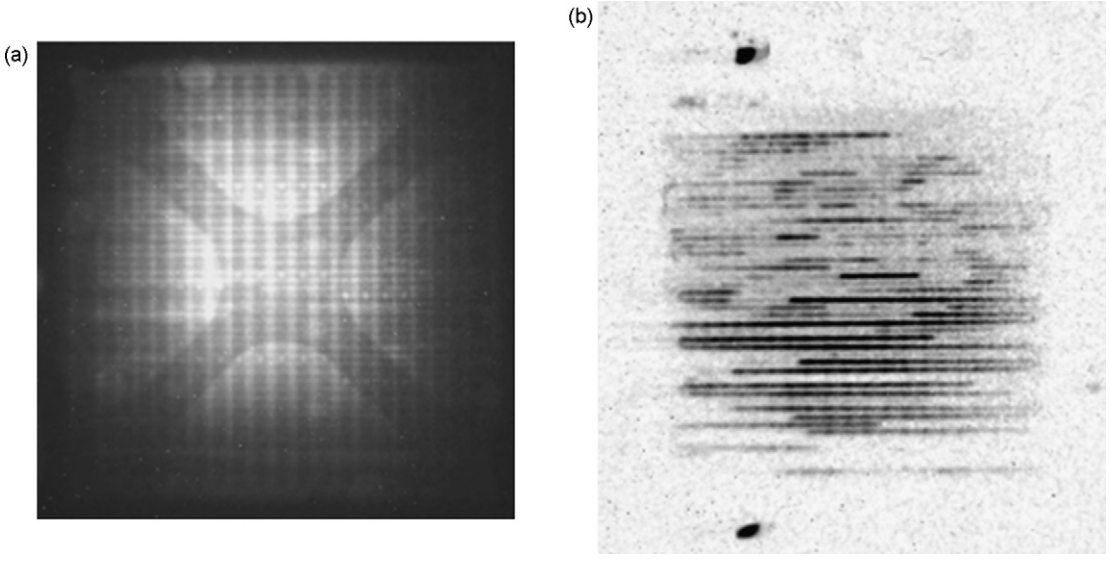

Fig. 2. (a) Radiograph as obtained from the experiment; horizontal lines denote the flowfield channels, vertical lines the contacts of the circuit board and the cooling flowfield. (b) Normalized image: liquid water can be identified as black lines and spots in the flowfield channels and the gas diffusion layer.

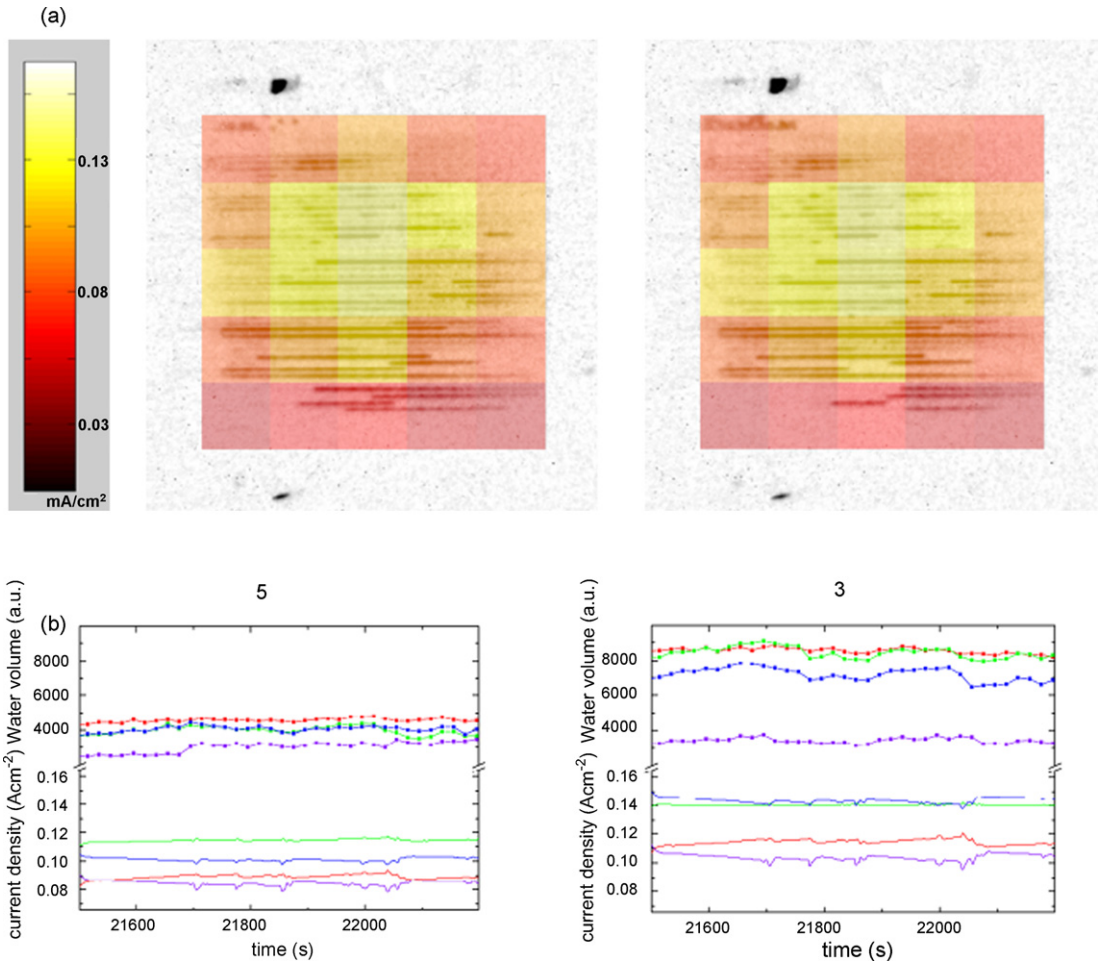

Fig. 3. (a) Water distribution and corresponding current density at cell current $I = 100\,\mathrm{mA\,cm^{-2}}$. The time distance between the two images is 600 s. (b) Water content (arbitrary units) and respective current density of the segments as denoted in Fig. 1.

evenly distributed over the whole active area with some (partially) flooded channels, which can be identified by dark lines. As determined from the flow directions of the reactant gases, the flooding occurs predominantly on the anode side, which was observed already by other groups [12]. At first glance, the current density distribution is, similar to the water distribution, quite uniform with its maximum density in the center of the cell; this maximum is caused by an interplay of several factors such as flow dynamics, cell design and electric contact. In the center, almost laminar flow conditions can be reached leading to a perfect supply of the reactive area. Due to the design of the end plates, the compression and therefore the electric conductivity reaches its optimum in the center of the cell. Reduced current densities in the lower part result from a depletion of the reactant gas hydrogen, which is fed on the 'top' of the flowfield with the outlet at the bottom. As the anodic utilization ratio is set to $u_A = 80\%$, the remaining concentration close to the outlet is not sufficient to reach comparable current densities as in earlier stages of the flowfield.

The total volume of the liquid water agglomerates and its correlation with the current density is tracked in more detail in Fig. 3b. Relative values along one row are considered to track changes along the reactant pathway. The hereby used colors correspond to the respective segment rows in Fig. 1a; the numbering of the plots denotes the segment column in Fig. 1a. Exemplified two columns are chosen which represent the whole system adequately. The variations in the local current densities are at this current load small between the segments along the vertical axis. Differences lie within a range of $0.05\,\mathrm{A\,cm^{-2}}$, across the active area the densities are in between 0.13 and $0.2\,\mathrm{A\,cm^{-2}}$. As evident from the neutron radiographies the uniform water distribution in the border segments of the active area is reflected in the quantified water volumes which all lie within a 10% range (column 5). In the central column, the water distribution is not as uniform any more with a clear trend towards increased amounts of liquid water in the lower fields. At the given operating conditions, however, a non-uniform water distribution does not affect the performance of the cell and the measured current densities are within the same range. It is remarkable that the lowest amount of liquid water does not correspond to the highest current density, which one might expect from a humidification point of view and gives a hint on a possible drying of the membrane.

At an average current density of $i_0 = 500\,\mathrm{mA\,cm^{-2}}$ the water distribution is not as uniform as at lower currents; furthermore, the maximum of the current density distribution is shifted slightly upwards compared to operating conditions with

$i_0 = 100\,\mathrm{mA\,cm^{-2}}$ (see Fig. 4a). In the lower part of the flowfield, an increased amount of liquid water can be observed; in the lowest section of the fuel cell the liquid water content is decreased again as at the cathodic inlet the back-diffusion is reduced due to the minor humidification of the reactant gas. The quantification of the water agglomerates in Fig. 4b corroborates this trend, where the same segments as in Fig. 3b are chosen. From a current density of $i_0 = 500\,\mathrm{mA\,cm^{-2}}$ onwards, the importance of a well-balanced water management becomes evident as can be easily identified in Fig. 4b. In segment column 5 (as denoted in Fig. 1b) the respective current density distribution is not as close as it was the case at lower currents (compare to Fig. 3b). The water distribution also shows a clear trend that is related to the current output: neither the lowest nor the highest water content lead to the best performance but an intermediate humidity gives the highest current output. From a certain water content onwards the power outage decreases in the lower part of the cell and the combination of excessive liquid water and depletion of the reactant gas leads to a reduced current density compared to the central segments. In the topmost segment, the amount of water is apparently not sufficient to fully humidify the membrane and the performance is also reduced compared to the segments below. In the central segments (column 3), the effects of the misbalanced water management is even intensified (Fig. 4b); the lowest and the highest water amounts are both correlated to reduced current densities.

From $i_0 = 500$ to $i_0 = 700\,\mathrm{mA\,cm^{-2}}$ the current density distribution becomes even more diverse (Fig. 5a). The flowfield channels in the lower third of the active area are more or less flooded leading to a decreased performance in the area under the respective segments. The time dependency of the current densities and of the water content are not as uniform as at lower currents. In the center, the distribution is even more irregular as in the border area; the maximum and minimum of the current density differ by almost 100% (Fig. 5b). The fluctuating water content in those segments is related to a noisy current density distribution as function of time. Larger water drops 'rushing' through the channels cause irregularities of the supply and lead in turn to changes in the current output. A detailed examination of the short-term effects of water droplets migrating through the flowfield channels will be performed in the following section. In the topmost segments, where effects of the insufficient humidification are easily identified by means of the water quantification curve, the time dependency of the current density is quite regular as there are no perturbations stemming from water droplets.

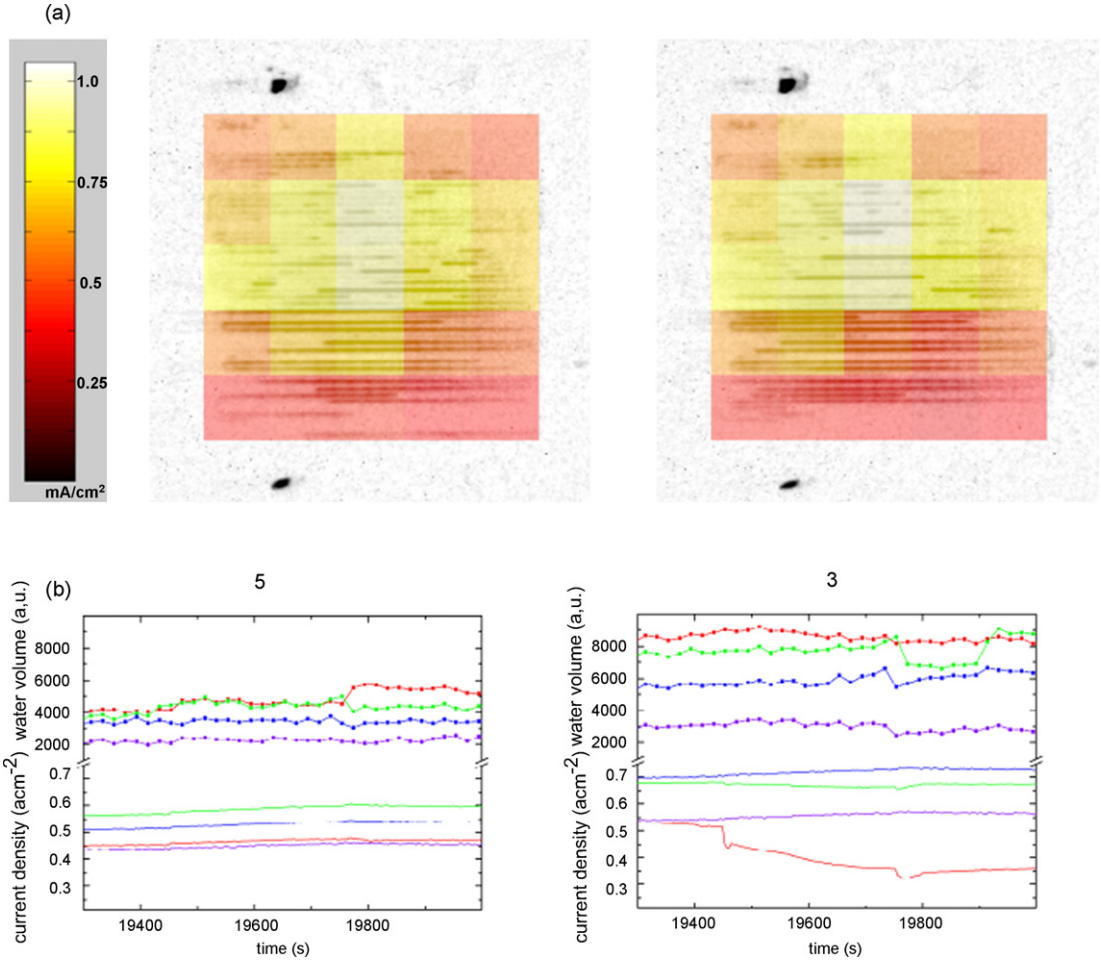

Fig. 4. (a) Water distribution and corresponding current density at cell current density $i_0 = 500\,\mathrm{mA\,cm^{-2}}$. The time distance between the two images is 820 s. (b) Water content (arbitrary units) and respective current density of the segments as denoted in Fig. 1.

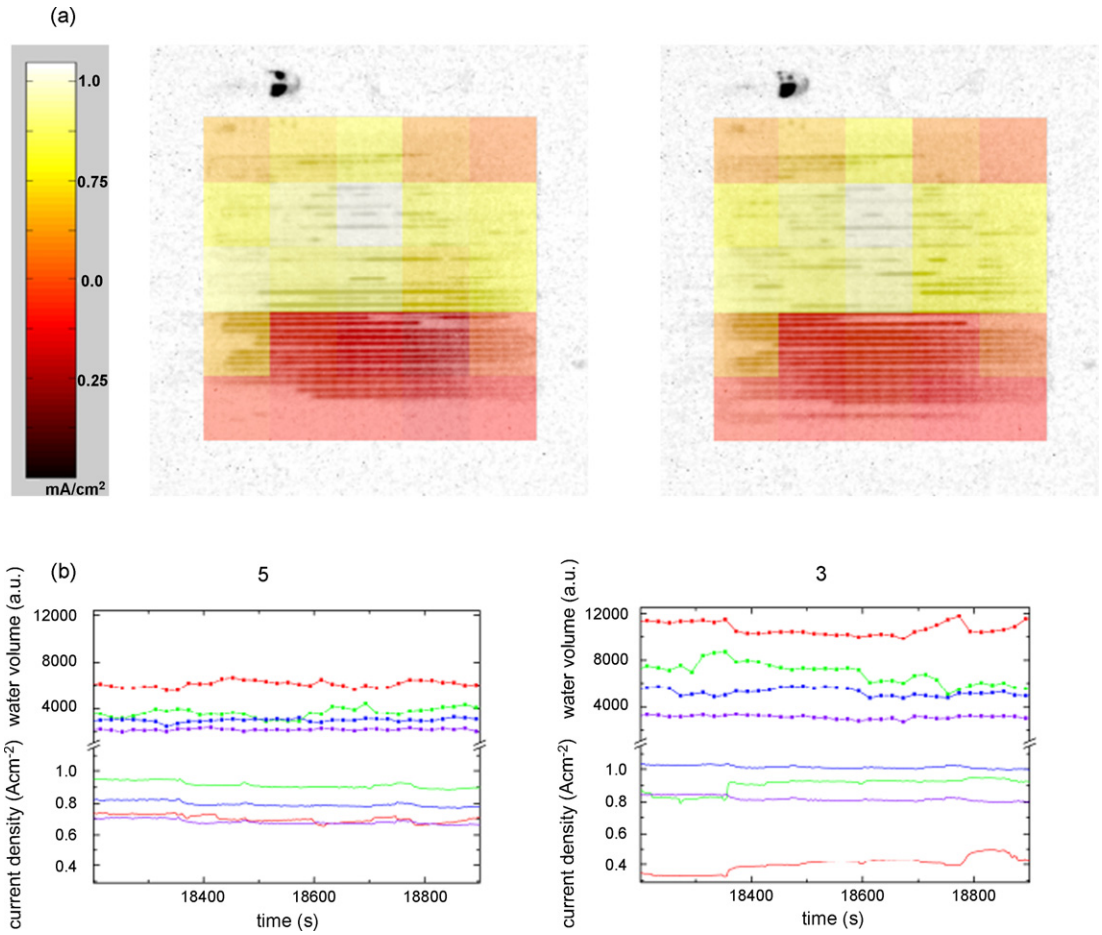

Fig. 5. (a) Water distribution and corresponding current density at the overall current density $i_0 = 700\,\mathrm{mA\,cm^{-2}}$. The time distance between the two images is 800 s. (b) Water content (arbitrary units) and respective current density of the segments as denoted in Fig. 1.

The short-term response of the local performance on water droplets migrating through the flowfield channels is studied in more detail on basis of single images instead of averaged water contents, which are used to describe the long-term behavior. In Figs. 6 and 7, two examples of fast activity responses in a distinct area on a water droplet passing through an adjacent gas channel are given. As demonstrated before, at an average current density of $i_0 = 700\,\mathrm{mA\,cm^{-2}}$, the local current density is not as uniform as at lower power requests. Not only in the lower third but also in the horizontal midfield of the considered segments several channels are at least partially flooded causing an undersupply of the reactive area. In the left image of Fig. 6a, the overall water content in the highlighted segment is high due to up to five flooded channels resulting in a reduced current density; after 10 s (right image of Fig. 6a), the water is transported away from this position (and away of this segment) and the normal supply of reactant gases is restored. The local current density returns back to its original (higher) value as is also illustrated by the color change of this segment. The reduction of liquid water in this field is additionally monitored by means of the quantified water content. Coinciding with the decreasing water content at $t \approx 18{,}350$ s, the current density is increasing abruptly. These sudden changes in the water content and the current density (spikes in Fig. 6b) typically result from small pressure changes caused by blocked channels, which are emptied if the pressure drop becomes too large.

In Fig. 7, the opposite situation compared to Fig. 6 is described, the immediate response of the local performance on a droplet 'entering' the segment. With the droplet becoming visible in the time dependent water content, the current density of this segment is decreasing as well. Thereby, the incoming droplet blocks the channel and the supply of reactant gases is stopped. Effects like cross-flow from a neighboring channel as well as cross-diffusion within the gas diffusion layer avoid a complete blockage of this area, however, the current density decreases by 10–20%. The droplet is not immediately transported away but the water content decreases slowly, indicating either a slow evaporation of the liquid water or a slow transport of water inside the gas diffusion layer, which accumulates inside if there is no other way to enter the blocked channel. As images were taken every 2 s, a time uncertainty is inherent in these images, which might camouflage a slight delay of the performance response on the blocked channel.

4. Discussion

Combined neutron radiographic imaging and locally resolved current density measurements were used to investigate the water

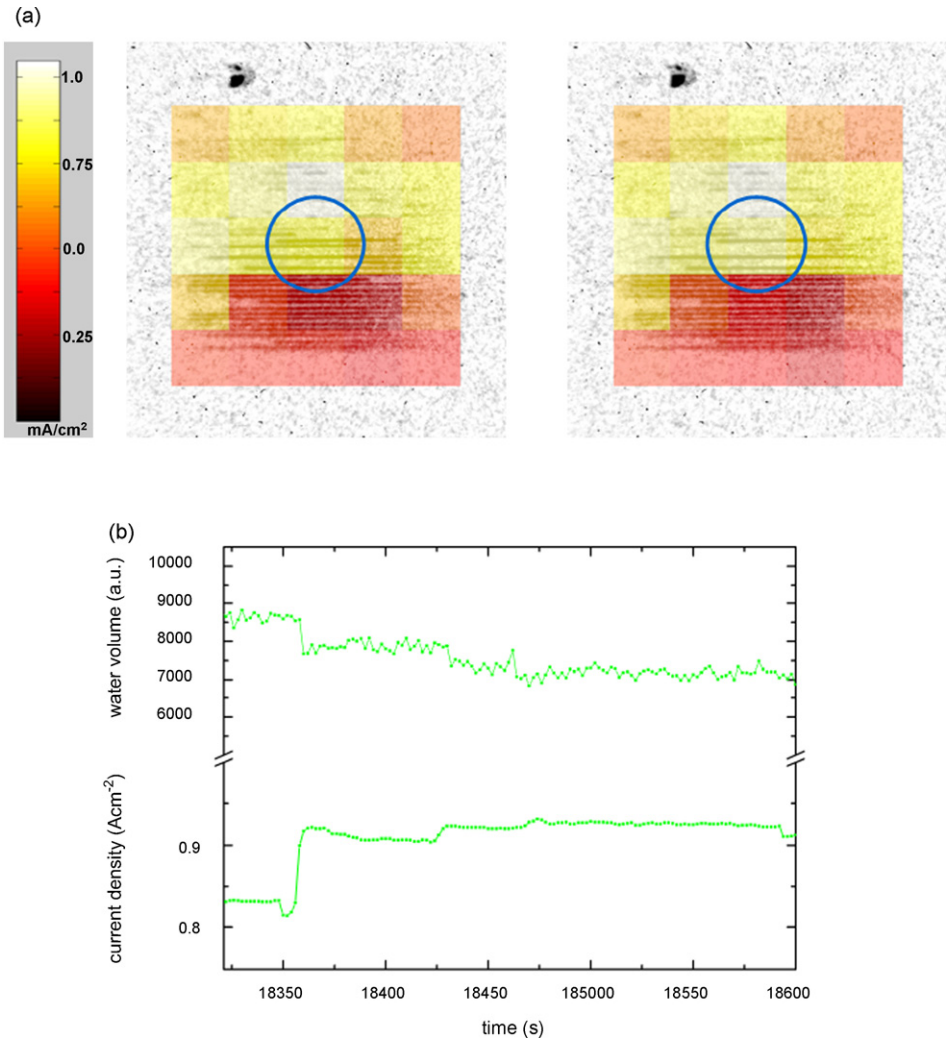

Fig. 6. Short-term response of the local current on changes of the water content in the channel. (a) Neutron radiographic images taken within an interval of 10 s to render migrating droplets in the channel. (b) Water content and current of the respective segment; after the disappearance of the droplet the current density increases again.

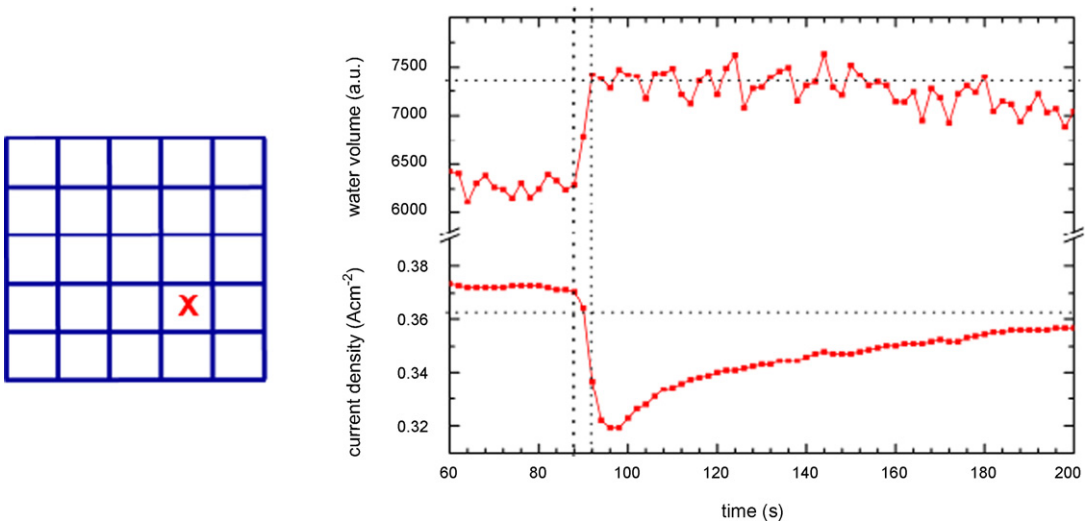

Fig. 7. Short-term response of the local current on changes of the water content in the channel. Left: considered segment of the electrochemically active area. Right: water content and current density in the respective segment at an overall current density of $i_0 = 500\,\mathrm{mA\,cm^{-2}}$; the appearance of the droplet leads to a sharp decrease of the local current density which recovers slowly when the overall water content decreases again.

management in an operating fuel cell equipped with a current density measurement board. The reactant gases were fed in counter flow mode with humidification on the cathode side. This setup should allow for a uniform distribution of water with the anode inlet next to the cathode outlet so that effects like back-diffusion can support the equal distribution of liquid water.

At low power requirements (average current densities in the range of 100 mA cm^{-2}) the water as well as the local current density distribution is quite uniform over the electrochemically active area. Some of the flowfield channels are filled with water, whereas an undersupply of the reactive area is not very likely since the distribution of current densities is very narrow, bearing only minor deviations. In contrary, most probably these agglomerates do not block the entire channel cross-section but fill the channels partially leaving enough space for reactant gases. With increasing performance requirements ($i_0 = 500$ mA cm^{-2}) two effects can be directly observed: the maximum of the local current density shifts closer towards the anode inlet and in the region close to the anode outlet performance losses were observed. The latter ones are caused by a combination of reactant gas depletion and first stage flooding effects. Most of the liquid water is observed in this area, hindering the reactant supply and leading to reduced local current densities. The minimum water content at this current is observed in the upper part of the cell; the performance of these segments is somewhat lower than in the central parts, indicating an insufficient humidification of the membrane. This effect becomes more prominent at higher currents ($i_0 = 700$ mA cm^{-2}) where a further performance decrease in the upper area is observed. Similar results were reported recently by Scherer and coworkers using locally resolved impedance spectroscopy [17]. Excess water on the anode agglomerates in the lower part of the flowfield where single channels of the flowfield are completely blocked and the performance in this part is drastically reduced. A more balanced water management might be achieved in such cases with thinner membranes, enhancing effects like back diffusion to equalize excess water on the one side and drying on the cathode side [19].

Besides long-term changes of the water distribution and the correlation with the overall performance, the short-term influence of single water droplets in the flowfield channels on the local current density has been studied. Small agglomerates are able to block at least partially the channel cross-section, causing a decrease of the performance when two adjacent channels are affected. As soon as these droplets are removed, the performance recovers and the current density reaches again the liquid free value. Effects of water droplets migrating through the channel were analyzed on this basis: the blocking effects step in immediately as a droplet is formed or (in our case) enters the area of the respective segment of the circuit board. The reactant supply is interrupted and the current density decreases sharply. The performance recovers slowly as an effect of cross-flow from channel to channel and cross-diffusion within the gas diffusion layer.

5. Conclusion

In conclusion, neutron radiography is a unique tool to investigate water distribution in unmodified, operating fuel cells. In combination with a synchronous measurement of the local electrochemical performance, not only excess water but also a lack of humidification can be detected and much more details causing performance fluctuations can be investigated. Variations of membrane and gas diffusion layer materials as well as different flowfield designs can be studied and their influence on the performance can be investigated which opens a wide field for optimization of low temperature fuel cells.

Acknowledgements

CH would like to thank the Fuel Cell Alliance Baden-Württemberg (FABZ) and the Deutsche Forschungsgemeinschaft (Le 1433/1-1) for financial support. This project was co-financed by the European Union and the City State of Berlin (EFRE 2000 2006 2/16).

References

[1] F.-B. Weng, A. Su, C.Y. Hsu, C.-Y. Lee, J. Power Sources 157 (2006) 674–680.
[2] A. Su, F.-B. Weng, C.-Y. Hsu, Y.-M. Chen, Int. J. Hydrogen Energ. 31 (2006) 1031–1039.
[3] X. Liu, H. Guo, C. Ma, J. Power Sources 156 (2006) 267–280.
[4] P. Argyropoulos, K. Scott, W.M. Taama, Electrochim. Acta 44 (1999) 3575–3584.
[5] H. Yang, T.S. Zhao, Q. Ye, J. Power Sources 139 (2005) 79–90.
[6] A. Hakenjos, H. Muenter, U. Wittstadt, C. Hebling, J. Power Sources 131 (2004) 213–216.
[7] K. Tüber, D. Pocza, C. Hebling, J. Power Sources 124 (2003) 403–414.
[8] A. Hakenjos, C. Hebling, J. Power Sources 145 (2005) 307–311.
[9] M.M. Mench, C.Y. Wang, M. Ishikawa, J. Electrochem. Soc. 150 (2003) A1052–A1059.
[10] M.M. Mench, Q.L. Dong, C.Y. Wang, J. Power Sources 124 (2003) 90–98.
[11] M.M. Mench, C.Y. Wang, J. Electrochem. Soc. 150 (2003) A79–A85.
[12] N. Pekula, K. Heller, P.A. Chuang, A. Turhan, M.M. Mench, J.S. Brenizer, K. Ünlü, Nucl. Instr. Methods Phys. Res. A 542 (2005) 134–141.
[13] D. Kramer, E. Lehmann, G. Frei, P. Vontobel, A. Wokaun, G.G. Scherer, Nucl. Instr. Methods Phys. Res. A 542 (2005) 52–60.
[14] R.J. Bellows, M.Y. Lin, M. Arif, A.K. Thompson, D.L. Jacobson, J. Electrochem. Soc. 146 (1999) 1099–1103.
[15] R. Satija, D.L. Jacobson, M. Arif, S.A. Werner, J. Power Sources 129 (2004) 238–245.
[16] J. Zhang, D. Kramer, R. Shimoi, Y. Ono, E. Lehmann, A. Wokaun, K. Shinohara, G.G. Scherer, Electrochim. Acta 51 (2006) 2715–2727.
[17] I.A. Schneider, D. Kramer, A. Wokaun, G.G. Scherer, Electrochem. Commun. 7 (2005) 1393–1397.
[18] R. Eckl, R. Grinzinger, W. Lehnert, J. Power Sources 154 (2006) 171–179.
[19] I. Manke, Ch. Hartnig, N. Kardjilov, W. Lehnert, J. Banhart, Appl. Phys. Lett. 90 (2007) 184101.